Status Report to NASA Headquarters

Science Team Evaluation of the OMPS Limb Profiler

Pawan K. Bhartia[1] and Glen Jaross[1]

Jack Larsen[2], Al Fleig[3]

[1]Earth Sciences Division- Atmosphere
NASA Goddard Space Flight Center

[2]Science Systems and Applications, Inc.

[3]PITA Analytic Sciences

Contents

Executive Summary 3
1 Introduction 4
1.1 Background 4
1.1 Organizational History 4
1.2 Team Charter 4
1.3 Processing Status 4
2 Instrument Highlights 5
2.1 Sensor Design Summary 6
2.2 Radiance Gridding and Consolidation 10
2.3 Internally Scattered Stray Light 12
3 Limb Scattering (LS) Technique 12
4 Sensor Performance and Calibration 14
4.1 Measurement Noise 14
4.2 Stray Light 15
4.3 Wavelength Registration 17
4.4 Thermal Effects 19
5 Altitude Registration Error 21
6 Evaluation of OMPS LP ozone profiles 24
7 Path Forward 27
7.1 Data Release #2 27
7.2 One Year and Beyond 27
8 Recommendations 28

Executive Summary

Launched October 28, 2011 the Suomi National Polar-orbiting Partnership (SNPP) satellite carries an Ozone Mapping and Profiler Suite (OMPS) consisting of three instruments: Nadir Mapper (NM), Nadir Profiler (NP) and Limb Profiler (LP). This report provides background information on the LP instrument, provides an overview of the limb technique it uses, discusses the quality of data released on Nov 1, 2013, and describes the algorithm improvements that are being planned for the next release. The following is a summary of our key findings.

1.The OMPS LP instrument is performing according to specification with the exception of thermal effects that cause the image of the limb on the CCD to shift in both the spectral and vertical direction when sunlight heats the front optics in the northern hemisphere. The effect is small and correctable. Sensor stray light, a pre-launch concern, is behaving as predicted, which means that software corrections work well.

2. There has been limited experience, particularly in the US, with the limb scattering technique that the LP instrument employs. Our conclusion is that the technique is quite robust. It is already producing ozone profiles with roughly the quality of limb ozone instruments that have flown in space over the past 35 years. We expect that with further tuning of the algorithms, the quality of ozone data will be similar to that from Aura MLS. The instrument provides ozone profiles with ~2 km vertical resolution over the 10-60 km altitude range, which is a big improvement over the profiles produced by the SBUV/2 instruments that have been flying on NOAA polar orbiters since 1985. The technique is not affected by (altitude independent) radiometric change in the instrument, a feature it shares with occultation instruments.

3. Since the instrument measures diffuse radiation from the limb rather than an astronomical object, such as the sun, the altitude registration of the measurements along the limb has been a concern. Our experience suggests that an altitude registration technique for limb scattering instruments, called RSAS, proposed about two decades ago, works reasonably well. It provides ±300m accuracy in determining the tangent height in most latitudes, which translates to ±7% error in ozone density. While we are continuing to improve the accuracy of the RSAS technique, we are also looking at other promising techniques to validate and improve upon RSAS.

4. Limb-scattered radiation is affected by stratospheric aerosols. This effect needs to be corrected for accurate ozone retrieval. As a byproduct of this correction one also gets an aerosol vertical profile. OMPS LP appears to have higher sensitivity to stratospheric aerosols than CALIOP/CALIPSO, while agreeing reasonably well on the average. A recent achievement has been the detection of a very thin layer of dust at 30 km produced by the meteor that exploded over Siberia on Feb 15, 2013. OMPS LP has been able to track transport of this dust around the globe. With further development, the aerosol product from LP is likely to become scientifically as important as the ozone product.

5. We released radiances (Level 1) and ozone profiles (Level 2) to the public almost exactly 1 year post-launch. This initial product included first order corrections for tangent height and wavelength registration errors, but few other refinements. Ozone density comparisons with MLS are already within ±10% at most altitudes and latitudes. In our next release (mid-2013) we plan to improve altitude registration and refine the retrieval algorithm to minimize unphysical vertical structures in the ozone profile. We plan to also release an initial aerosol profile product.

1 Introduction

1.1 Background

This report details results of the work performed by the SNPP OMPS Limb Profiler (LP) Science Team to evaluate the overall performance of the OMPS LP instrument, L1 and L2 algorithms, and its potential to produce long term climate quality ozone profiles.

The OMPS LP instrument is designed to provide high vertical resolution ozone profiles with the limb scatter technique, continuing the long-term ozone profile data record begun by the Solar Backscattered Ultraviolet (SBUV/SBUV2) series of instruments, the Stratospheric Aerosol and Gas Experiment (SAGE I/II/II) solar occultation measurements, and the Microwave Limb Sounder (MLS). While the OMPS LP instrument uses the same limb viewing geometry as SAGE and MLS, the retrieval of ozone profile by the limb-scattered radiation is a relatively new technique with which there has been limited experience in the US.

1.1 Organizational History

The initial concept was that all three types of measurements from OMPS, nadir maps, nadir profiles and limb profiles would be part of the overall SNPP effort with algorithm development, maintenance and processing part of the prime contract. However, in 2006 the LP instrument was removed from the SNPP contract as a cost saving action. In 2007 it was returned to the mission as a NASA-NOAA joint research instrument with NASA responsible for the algorithm development and processing. An informal LP Team was assembled at NASA GSFC by combining several existing tasks. SNPP OMPS PEATE was given the responsibility of finishing the algorithms that existed at that time and for developing a data processing system. Calibration and Level 1 algorithm development effort is being led by Dr. Glen Jaross. Level 2 algorithm development was led by Dr. Didier Rault from NASA/LaRC. In 2012, after Dr. Rault retired from NASA, Dr. P.K. Bhartia from NASA GSFC, became the acting OMPS LP team leader.

Processing is being done in the (PEATE supported) Atmospheric Chemistry Processing System (ACPS) that also serves as the Science Investigator Processing System (SIPS) for OMI and supports GSFC's reprocessing of TOMS data into a consistent multi-instrument dataset. Dr. Curt Tilmes/GSFC led the development of the ACPS. He is currently on detail to the US Global Change Research Program, Dr. Albert Fleig provides the coordination between disparate components that have been cobbled together to create the LP algorithm development and processing system.

1.2 Team Charter

PEATE has full responsibility for monitoring and characterizing the OMPS LP instrument, ground processing, and instrument operations. The current algorithms for generating L1 and L2 products, aka SDR and EDR, are essentially the same as they existed prior to launch. Since PEATE doesn't have the resources to improve the L2 algorithm, the current focus is largely on improving the L1 algorithm and maintaining the L2 software. A separate small team managed by Dr. Bhartia is analyzing the scientific products and is improving the L2 algorithm. It is expected that this activity will transition to the PIs selected through the 2013 ROSES solicitation.

1.3 Processing Status

Although there was some initial concern about whether the processing effort would be resource constrained, this has not been the case. The system has sufficient capacity to support algorithm

development and will be able to reprocess data as new algorithm versions are approved. A provisional dataset was produced and released within six months of the start of regular operation of the instrument and data are currently being routinely processed as they become available from the Suomi NPP flight data system. Each year of data requires less than four weeks to reprocess from L0 to L2.

2 Instrument Highlights

The OMPS LP sensor images the Earth limb by pointing aft along the spacecraft flight path. Figure 2.1 shows a schematic of the OMPS viewing geometry. The tangent point of the sensor line of sight (the point where the line of sight intersects an Earth radius vector at a right angle) is approximately 25º in latitude to the south of the subsatellite point. The sensor employs 3 vertical slits separated horizontally to provide wider cross-track coverage. Full global coverage is obtained in 3-4 days (see Figure 2.2).

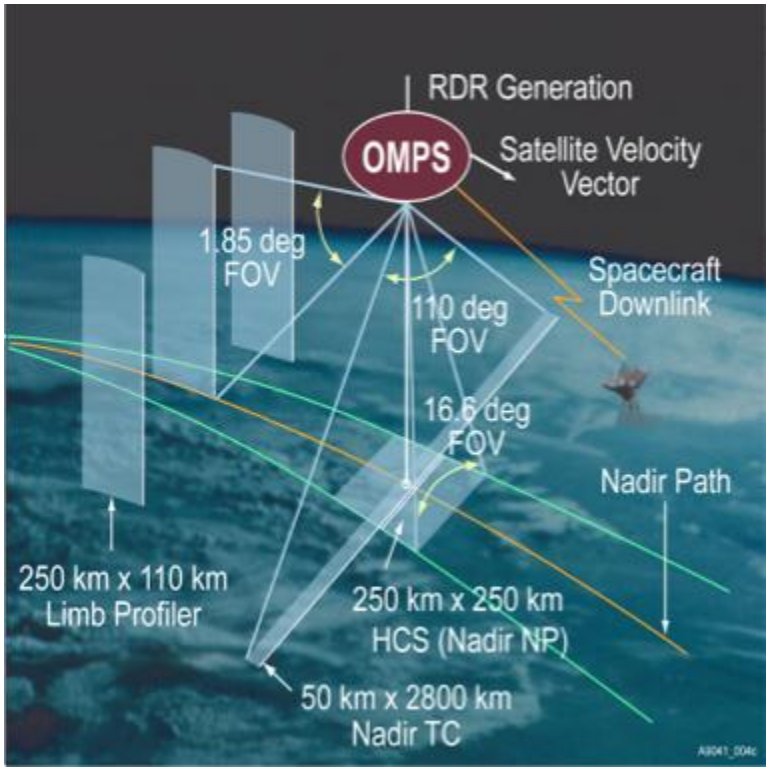

Figure 2.1: A schematic of the fields of view for the 3 OMPS sensors. The Limb sensor's 3 slits view approximately the same atmosphere measured by the Nadir sensors 7 minutes earlier.

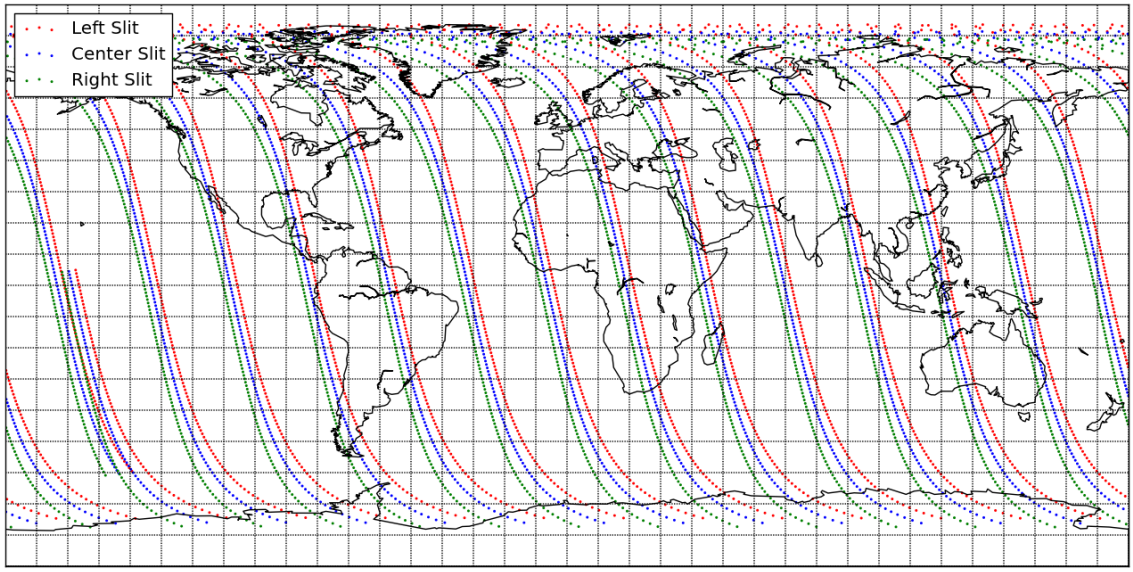

Figure 2.2: Tangent point latitude, longitude for the 3 OMPS LP slits over the course of 24 hours.

The instrument measures limb scattered radiances and solar irradiances at 220 wavelengths between 275 nm and 1050 nm. The measurement altitude range varies with latitude and season, but the 5-80 km range is always covered. The instrument currently collects data 6 days every week in the normal mode. On Sundays the Nadir instrument collects data at high spatial resolution and the Limb instrument collects an orbit at full spectral sampling. A decision whether to continue operating in this mode or to go to full 7 day/week operation hasn't been made.

2.1 Sensor Design Summary

During the OMPS development by the sensor vendor, Ball Aerospace and Technology Corp., a set of sensor specifications was derived that would allow the sensor suite to meet its ozone measurement requirements. Because the Limb sensor was only required to measure ozone concentrations between the tropopause and 60 km, several important simplifications could be made to the sensor design. Underlying the sensor design, shown in Figure 2.3, are several key concepts.

1. High spectral resolution is only needed for wavelengths shorter than 350 nm.
2. Use of a vertical scanning mirror is to be avoided for reliability reasons.
3. A modern CCD equipped with anti-blooming drains can be allowed to saturate without sacrificing the radiometric accuracy of nearby pixels.
4. Stray light can be controlled effectively through the careful application of cutoff filters at the focal plane.

The first of these concepts has led to the use of a prism rather than a grating disperser in the spectrometer. The prism provides 1 nm resolution needed for ozone spectroscopy at the Ultraviolet (UV) end of the sensor spectrum, and 30 nm resolution in the infrared (IR) where broadband radiometry suffices (see Figure 2.4). A design advantage resulting from the prism's

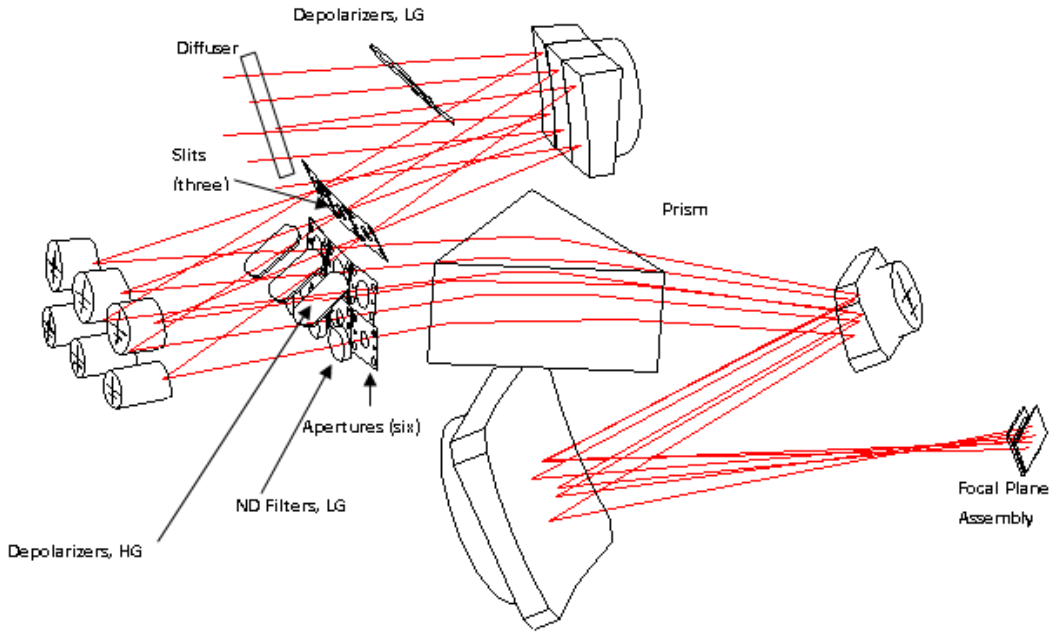

Figure 2.3: Optical layout of the OMPS Limb sensor. The telescope, which is upstream of the six entrance apertures, contains six corresponding mirrors that effectively "steer" images of the slits onto the single focal plane. (Figure courtesy of Ball Aerospace and Technology Corporation)

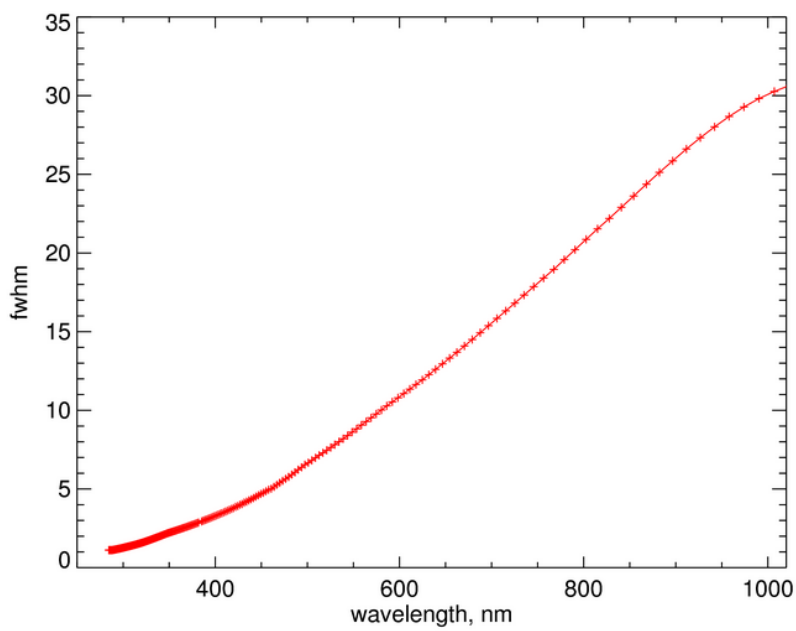

Figure 2.4: Full width at half maximum (nanometers) of the OMPS Limb slit function. The large variation with wavelength results from the highly non-linear dispersion of the spectrometer's prism. Each point represents a single pixel's band center and bandwidth.

highly non-linear dispersion is a reduction in detector size in the spectral dimension. A prism also generates less internal scattering than a traditional grating.

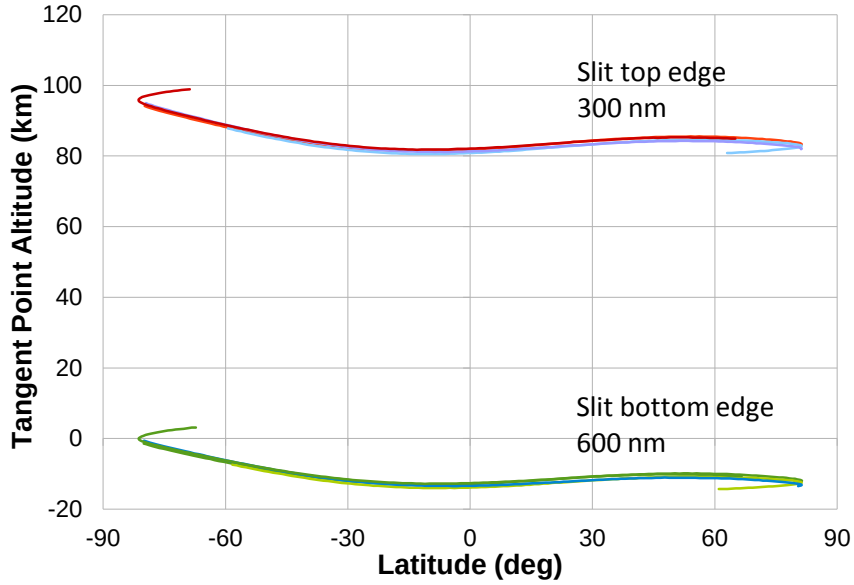

Figure 2.5: The extent of the vertical coverage of the center slit is shown as a function of latitude. Coverage varies slightly as a function of wavelength, so appropriate wavelengths are shown for the top and bottom of the slit image, which also comes from different apertures. The "hooks" at either end of the orbit represent variations toward solstice conditions.

Lack of a mirror to vertically scan the atmosphere means that a 2-dimensional detector must be employed to simultaneously capture the spectral dispersion and its vertical distribution. In the case of OMPS a CCD is used. Each of the 3 narrow vertical slits provides a 1.85° field of regard that views the Earth limb from the side. This vertical extent corresponds to 105 km at the tangent point. The slit heights are oversized to ensure coverage from the surface to 65 km as spacecraft nods up and down through the orbit. The full vertical coverage is shown in Figure 2.5.

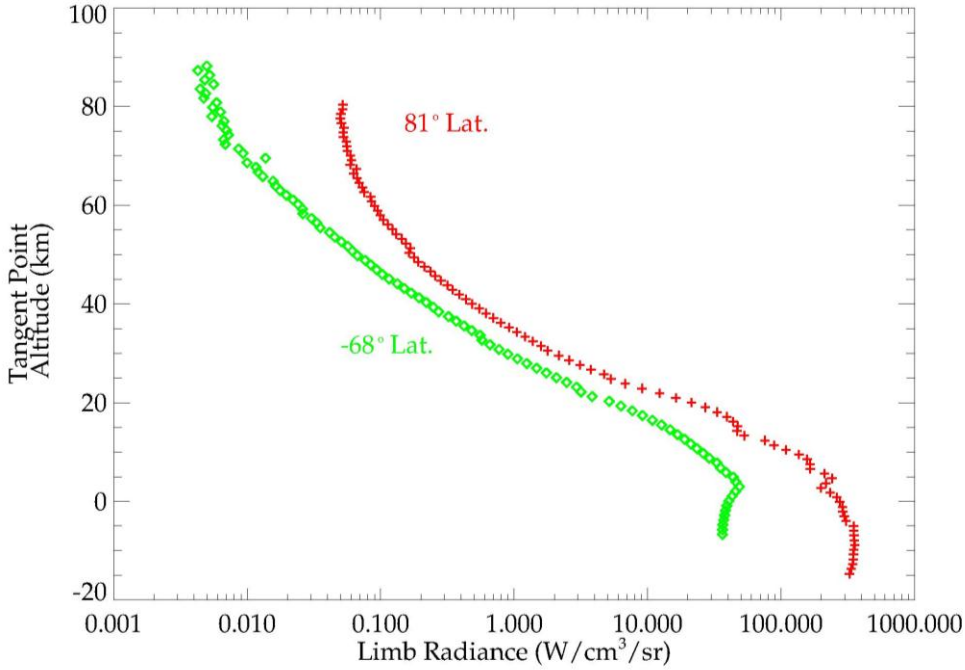

Figure 2.6: The limb radiances measured by OMPS at 890 nm on orbit 4110 exhibit the large dynamic range needed by the sensor.

Between the Earth's surface and a height of 100 km the limb scattered radiances in the IR decrease by at least 5 orders of magnitude as a result of decreasing particle density (see Figure 2.6). This dynamic range poses unique challenges when the radiances are measured simultaneously rather than sequentially, as when scanned. The well depth of a CCD is no more than $7 \cdot 10^5$ electrons, so gain settings that allow the lowest altitudes to remain unsaturated provide insufficient signal at high altitudes. Scanning instruments can extend their dynamic range by varying the integration time through the scan, but a fixed-imaging CCD cannot. One solution employed by OMPS is to collect interleaved images of the full atmosphere at two different integration times. These two integration times differ by a factor of 30. The sensor also increases dynamic range by collecting the full range of radiances simultaneously through a large and a small aperture. The aperture areas, and therefore the measured signals, differ by a factor of 2.8. Since each slit employs two apertures, a total of 6 full atmospheric spectra are imaged at the focal plane. The focal plane layout is shown in Figure 2.7. The multiple integration times, multiple apertures, and a 14-bit A/D converter give the sensor a dynamic range capability of $1.4 \cdot 10^6$. It remains for the ground processing algorithm to select the most sensitive, unsaturated signals and combine the multiple measurements into a single radiance profile.

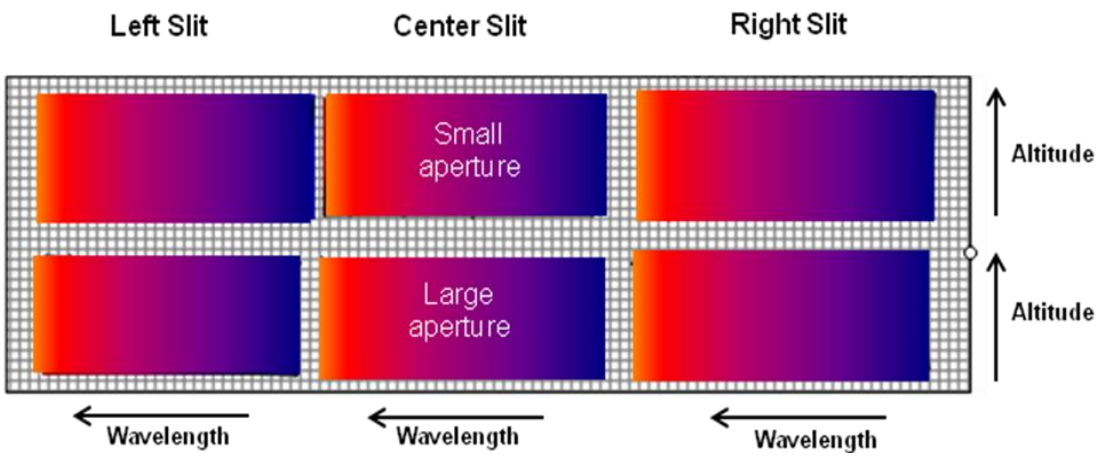

Figure 2.7: A schematic representation of the focal plane layout showing the six slit images (2 apertures for each of 3 slits). Each slit is tall but very narrow in the dispersion direction.

2.2 Radiance Gridding and Consolidation

As seen in Figure 2.8, data for each slit are collected in 4 gains (2 apertures, and 2 integration times) to cover the dynamic range of limb signals. In order to economically use the available data rate, pixel data are typically not collected at altitudes where they will saturate or where a higher gain is more appropriate. The current version of the ozone retrieval algorithm expects a single radiance value at each wavelength and tangent height, so the data processing code must combine the 4 radiance sets to obtain a self-consistent set of values covering the full tangent height altitude range. The uniform grid of detector pixels is not uniformly spaced in tangent height and wavelength, so the radiances must be transformed to such a grid. This transformation is currently performed using bilinear interpolation of measured radiances at each pixel.

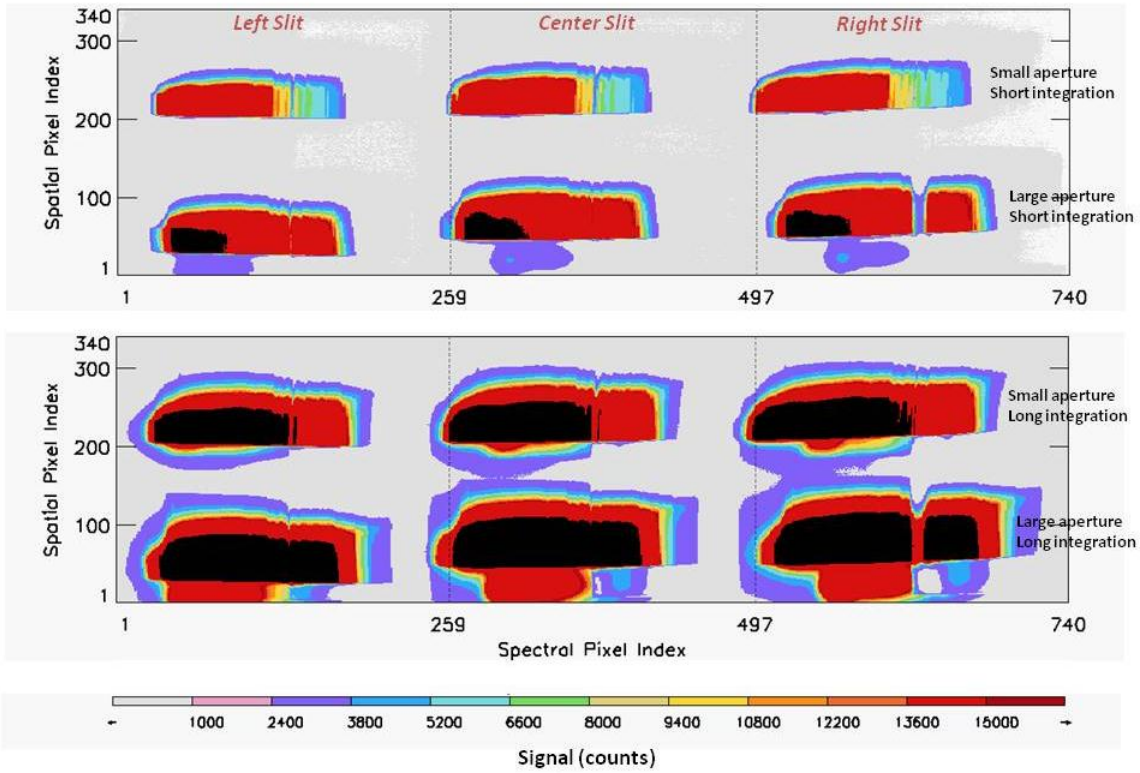

Figure 2.8: Information content available for each 19 sec. image of the atmosphere. Four sensor "gains" are used to cover the dynamic range of signals. The most sensitive of the gains is shown at the bottom of the image and the least sensitive at the top. Black indicates detector pixel saturation. The retrievals use data from the top row for the lowest altitudes of the atmosphere, and progress to the bottom row for the highest altitudes.

Radiances from the 2 different apertures can be combined once they are spectrally and spatially aligned. There are always small differences in the two sets of radiances due to stray light, ground calibration errors, interpolation errors, etc. Spatial overlap between adjacent gains can be used to assess these differences and remove them. This is important because the retrieval algorithm does not respond well to radiance discontinuities. The current processing code does not adjust radiances based on the observed difference. Rather, it performs a weighted average of the radiances at each grid point, where the weight is based on estimated radiance noise. The biases are removed only when their underlying cause is identified and corrected.

The largest radiance bias between the gains occurs as a result of vertical misregistration of individual detector pixels. Photons from a specific line of sight direction end up at a specific detector pixel based on the alignment of the sensor optics shown in Figure 2.3. Any change in that alignment following the pre-launch calibration of pixel pointing results in an error in the assigned tangent height for a given pixel. Furthermore, a change whose magnitude differs between large and small apertures will result in inconsistent radiances for the same tangent height. We believe that such an alignment shift has occurred (for more information see discussion in Section 4.4). The currently released product contains a constant adjustment to the

pointing biases between the large and small apertures. These adjustments (Left: 0.5 km; Center: 0.4 km; Right: 0.8 km) serve to correct tangent height errors as well as minimize radiance inconsistencies at different tangent heights.

2.3 Internally Scattered Stray Light

Spectral-spatial detectors such as on OMPS are more susceptible to internally scattered stray light because photons from bright parts of a scene can scatter both spectrally and spatially into weaker signal regions. In the case of the Limb sensor photons from low altitudes and at longer, unabsorbed wavelengths scatter diagonally into the weaker UV signals at high altitudes. Furthermore, with multiple images on a single detector, a significant portion of the stray light is inter-image. Photons from the IR portion of one slit can scatter into the UV portion of its neighboring slit, and vice versa.

The OMPS Limb approach to dealing with stray light is twofold: optical filtering and signal correction during ground processing. A visible blocking filter is applied to the focal plane window for those portions of the detector that collect light shorter than 370 nm. The physical edge of the filter is matched to its cutoff wavelength so that visible light incident on the visible wavelength portions of the detector is unaffected. This alone significantly reduces stray light in the high altitude UV wavelengths. The UV data are used for ozone retrievals at altitudes above approximately 35 km. Stray light point spread functions (PSFs) were also extensively measured during sensor ground testing. During these tests a tunable laser was used to create a series of spectral/spatial point sources. The full detector response, or PSF, to each point source was measured down a level of 10^{-9} times the source signal. A 4-dimensional stray light Jacobian was constructed by interpolating these measured PSFs to intermediate source wavelengths and altitudes. This Jacobian, which describes the amount of stray light in pixel i attributed to a source with measured signal in pixel j, is the basis for subtracting the stray light portion of the measured Earth limb signals.

3 Limb Scattering (LS) Technique

The limb scattering technique shares many common features with other limb-viewing ozone profiling techniques, including occultation methods. Here we highlight some of the key differences. Figure 3.1 provides a simplified diagram of the path of the solar radiation from the vantage point of someone looking at the earth from an inertial reference frame. A key difference from other techniques is that in LS the solar radiation enters the line of sight (LOS) from outside and gets scattered into the LOS, mostly by Rayleigh scattering, but sometimes by clouds and aerosols when they are present along the LOS. For occultation techniques, the source of the radiation is to the left end of the LOS, and for thermal emission techniques the radiation is generated by the ozone molecules along the LOS. Since the solar radiation coming from above the LOS can be modeled accurately, this difference, in itself, doesn't introduce any additional complexity for retrieving ozone profiles from LS. However, at longer wavelengths (λ>300 nm) one also gets diffuse upwelling radiation (DUR) coming from below the LOS that gets scattered into the LOS. Since there is very little atmospheric scattering in thermal IR and virtually none in microwave, this is usually not a problem at these wavelengths except when there are clouds along the LOS.

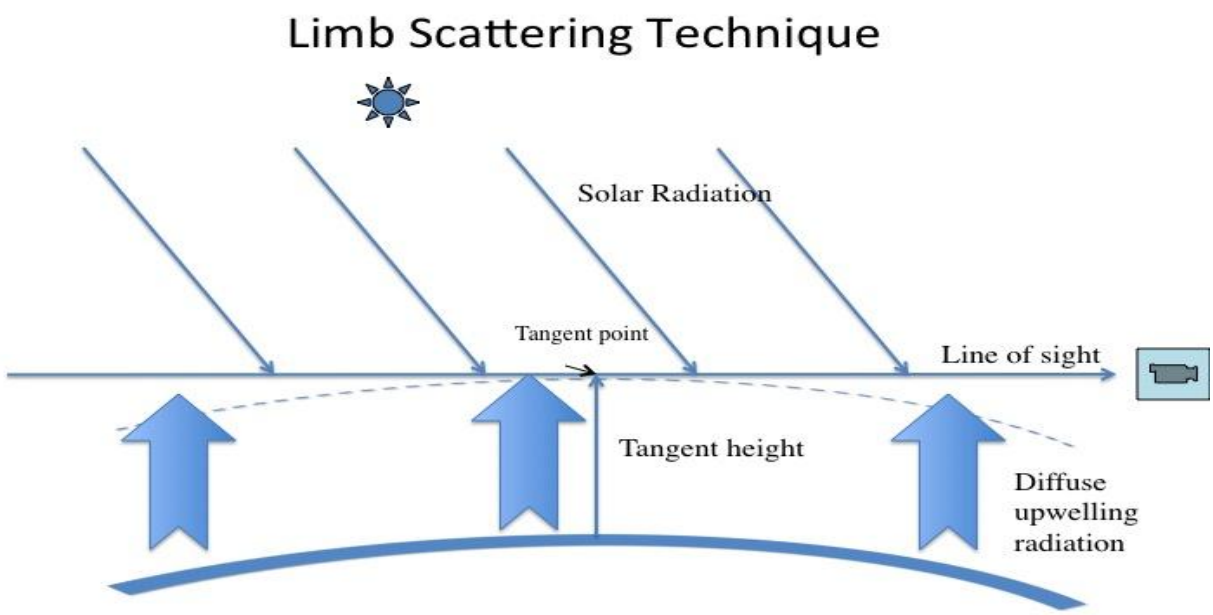

Figure 3.1: Schematic of the limb viewing geometry showing the primary sources of radiation, solar and diffuse upwelling radiation, observed at the instrument.

The DUR is generated by scattering of solar radiation from below the LOS by Rayleigh scattering, clouds, aerosols and earth's surface. It is the radiation that a nadir-viewing sensor measures when it reaches the satellite altitude. At visible wavelengths DUR from bright clouds can become equal to the solar radiation coming from above the LOS. However, there is no practical way of estimating the DUR in the visible, since the radiation comes from clouds from 2π solid angle under each point along the LOS. At the UV wavelengths the Rayleigh contribution can be estimated accurately but not the cloud contribution, which starts to become significant at λ>310 nm. The LS algorithms solve this problem by taking advantage of the fact that at the longer wavelengths DUR varies relatively little with altitude after it enters the stratosphere. Therefore one can remove most of it by high altitude normalization, i.e., dividing the radiation at altitude z with the radiation measured at a higher altitude where the ozone absorption at that wavelength is small. The small DUR variation can be accounted for by estimating an effective albedo of the scene from measurements at a non-absorbing wavelength(s). This approach also makes the LS technique "self-calibrating" since the normalization also removes any changes in (altitude independent) radiometric sensitivity (measured count/photon) of the instrument.

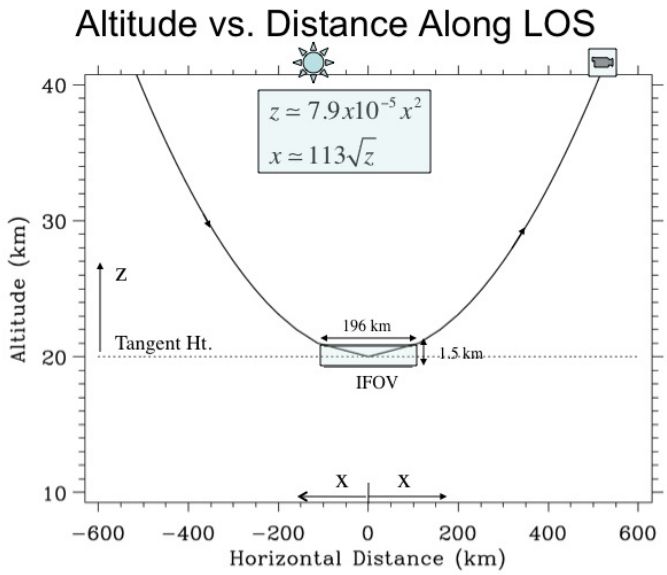

Figure 3.2: Schematic diagram showing how the radiation source region varies with altitude along the line of sight.

The path of the radiation from the vantage point of a person standing under the tangent point (TP) is shown in Figure 3.2. The LOS follows a parabola that rises up as one goes away from the TP in either direction. In a 1.5 km vertical field-of-view of the instrument, one receives radiation from a ~300 km horizontal distance. This is roughly the horizontal and vertical resolution of LP profiles. However, the radiation received from this box is affected by ozone molecules outside the box. One can remove this contribution either by "onion peeling" (retrieving from the top and going down) or using a first guess profile that is iteratively modified simultaneously at all altitudes. The latter method is used for LP. Either method works well above the ozone density peak since the number of ozone molecules outside the box decrease very rapidly with altitude. This is because of two effects: decrease in horizontal distance along the LOS with z plus a ~22%/km decrease in ozone density. However, below the density peak the two effects go in the opposite direction. This reduces the accuracy and precision of ozone profiles retrievable from most limb-viewing instruments. For limb scattering techniques there is, however, a 3rd effect that can potentially reduce this error. This effect comes from ~14%/km, decrease in Rayleigh scattering. However, it is too early to tell if we can take advantage of it to produce better ozone profiles below the peak from LP compared to previous limb sensors.

4 Sensor Performance and Calibration

4.1 Measurement Noise

Estimates of sensor measurement noise are shown in Table 4.1 for three separate tangent point altitudes. Each table contains three noise values: the level specified in the sensor design, a statistical estimate based on observed detector signal levels, and the observed standard deviation of radiances. In general signals become weaker with increasing altitude, resulting in smaller signal-to-noise ratios (SNR). But because the instrument has two apertures that independently

collect photons over the full wavelength and altitude range at two integration times, higher altitude signals at some wavelengths can actually be less noisy than lower altitude ones.

15km tangent point				30 km tangent point				60 km tangent point			
Wave-length	Spec. SNR	Obs. SNR	Radiance Noise	Wave-length	Spec. SNR	Obs. SNR	Radiance Noise	Wave-length	Spec. SNR	Obs. SNR	Radiance Noise
900 nm	1860	970	305	**900** nm	555	610	120	**353** nm	445	470	675
750 nm	1860	820	250	**750** nm	1170	1065	575	**320** nm	350	415	395
602 nm	1860	1845	1365	**602** nm	1805	660	790	**310** nm	295	355	290
500 nm	2430	2010	1830	**500** nm	1870	860	970	**302** nm	230	315	285
430 nm	2150	1590	1455	**430** nm	1870	835	730	**296** nm	220	295	180
353 nm	2650	930	970	**353** nm	2380	645	550	**290** nm	190	300	190

Table 4.1: Comparisons of expected and observed sensor noise. The first column is expected detector noise, the second is calculated noise from actual measurements, and the third is based on observed radiance variance.

In comparing the two noise measures to the design values it is first of all apparent that the measurements yield lower SNRs. This is to be expected because the design assumed optimized pixel well-filling for any given measurement, something that seldom occurs. But observed detector SNR does generally follow the design since modeled signal levels were reasonably accurate. Radiance noise tends to have the lowest SNR of the three because it is impossible to eliminate all true, geophysical variations from the estimates. Such variance tends to occur at low altitudes and long wavelengths.

4.2 Stray Light

It has been noted that internally scattered stray light is a significant error source common to all limb scatter measurements, but especially in the OMPS design. A stray light Jacobian derived from measured PSFs is used to estimate and subtract the stray light content of every scene. This works in so far as the PSFs were accurately measured and all stray light sources are available in the data record. If, as is the case with OMPS, not all pixel signals are sent to the ground, then these missing sources must be estimated. Fortunately, no significant stray light sources lie outside the measurement range of OMPS Limb, so interpolation between measurements is a sufficiently accurate form of estimation.

The projected stray light levels from the original sensor design are given in Table 4.2. Using the stray light Jacobian, the in-flight stray light content is estimated and removed from each image during ground processing. An example of the content for the center slit, large aperture image is shown in Figure 4.1. Stray light percentages in other slits and apertures are similar but not identical. Table 4.2 and Figure 4.1 compare remarkably well. As this figure also confirms, stray light is primarily a high altitude problem, though levels are less than 10% at most altitudes. Stray light tends to increase with wavelength for a given tangent point altitude, an effect caused by the greater signal gradient with altitude at long wavelengths. Lower Rayleigh scattering cross

sections mean that limb radiances in the visible and infrared vary more in proportion with atmospheric density. The left slit IR wavelengths and right slit UV wavelengths have less stray light because these regions are at the detector edge and don't receive scattered photons from neighboring slits.

Wavelength	**15** km	**35** km	**45** km
900 nm	1.0	6.2	14.0
750 nm	0.5	2.5	5.3
602 nm	0.5	1.3	2.6
500 nm	0.5	0.8	1.6
430 nm	0.5	1.0	2.0
353 nm	0.5	0.5	0.5

Wavelength	**45** km	**52** km	**65** km
353 nm	0.5	0.6	1.7
320 nm	0.5	-	2.7
310 nm	1.2	-	5.3
302 nm	2.7	2.9	7.5
296 nm	-	3.4	7.4
290 nm	-	5.5	8.5

Table 4.2: Percent stray light amounts predicted pre-launch for the OMPS Limb sensor. These values are prior to any correction in ground processing.

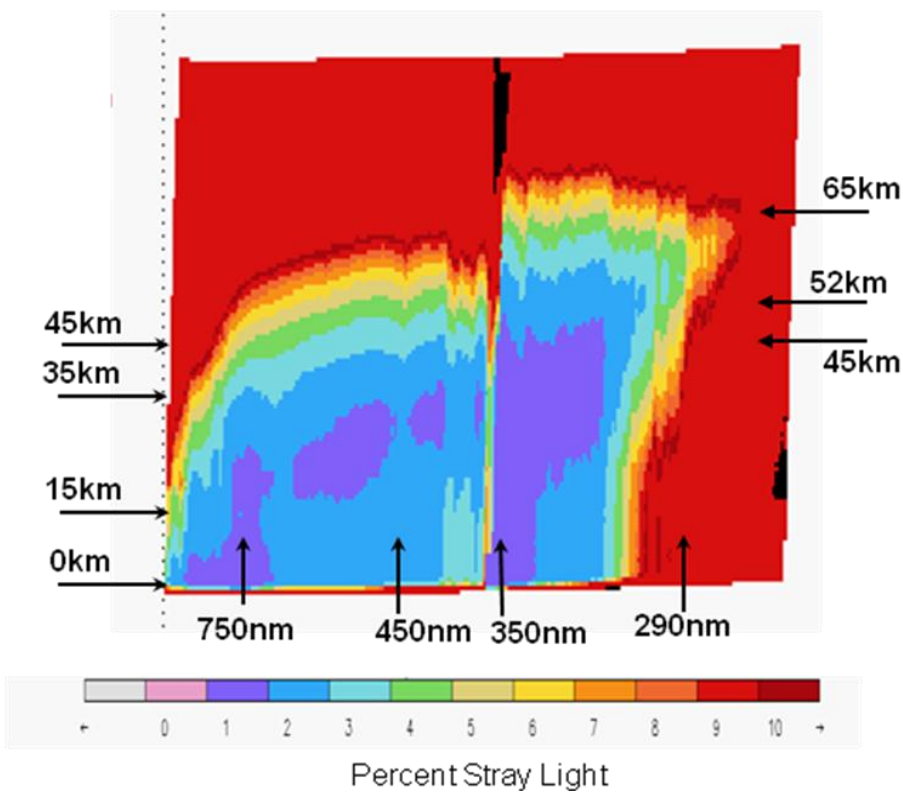

Figure 4.1: Calculated stray light (orbit 1449) based on the measured limb signal in the center slit, large aperture and the OMPS stray light model.

An estimate of the accuracy of the stray light model and associated corrections is obtained by observing dark areas of the detector. The six images shown schematically in Figure 2.7, referred to as the optical region, are the only areas of the detector that receive direct photons. Any

photons collected outside this region were scattered there. Figure 4.2(a) shows detector signal levels for a typical Earth limb scene along with the approximate outlines of the image region. The non-zero signal levels outside the optical region are a clear indication of scattered light. After subtracting the estimated stray light signal, the remainder is shown in Figure 4.2(b). A perfect correction of stray light would result in grey or black colors surrounding the entire optical region. This occurs only for high altitude UV signals (right side of image). In the visible and IR regions the correction is poorer in terms of absolute signal, but as a fraction of the total signal the stray light levels there are already small. The one exception is in the extreme IR (far left of the image), where residual errors can exceed 10%.

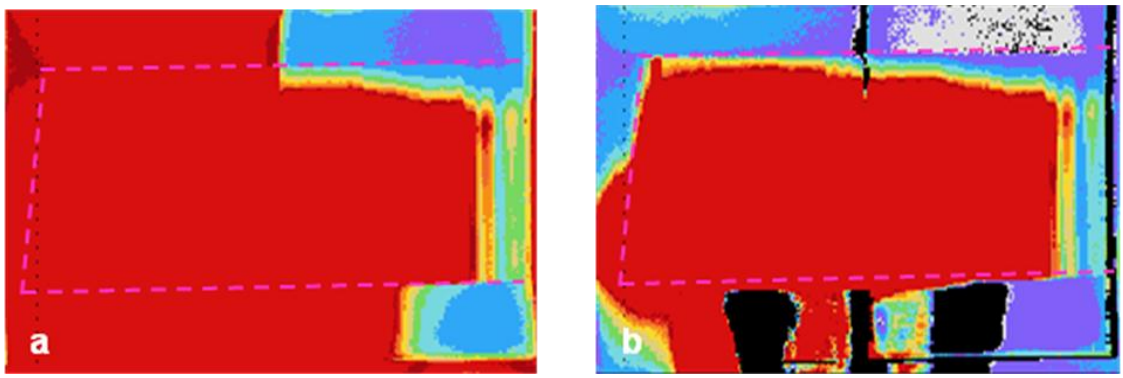

Figure 4.2: Signal levels in the center slit, large aperture image are shown for (a) uncorrected signal, and (b) stray light portion of signal removed. The physical outline of the detector optical region in shown as a dashed line. Black areas in (b) indicate negative counts, where an over-correction occurred.

4.3 Wavelength Registration

The regression of a measured solar spectrum with a well-known reference spectrum has become the standard technique for determining band center wavelengths of hyperspectral sensors, and can be performed using either measured solar irradiance or backscattered Earth radiance. Uncertainties of 0.01 spectral pixels are typically obtained for the GOME and OMI instruments using this technique. Results from OMPS Limb solar measurements have approximately 0.01 nm uncertainty at 300 nm and nearly 0.5 nm toward the IR end of its spectrum. This is in line with the historical 0.01 pixel value.

Figure 4.3 contains a comparison between the registration obtained post-launch using OMPS solar measurements and that characterized on the ground by the sensor vendor. The solar spectrum approach is generally more accurate than pre-launch characterizations that use laboratory lamps.

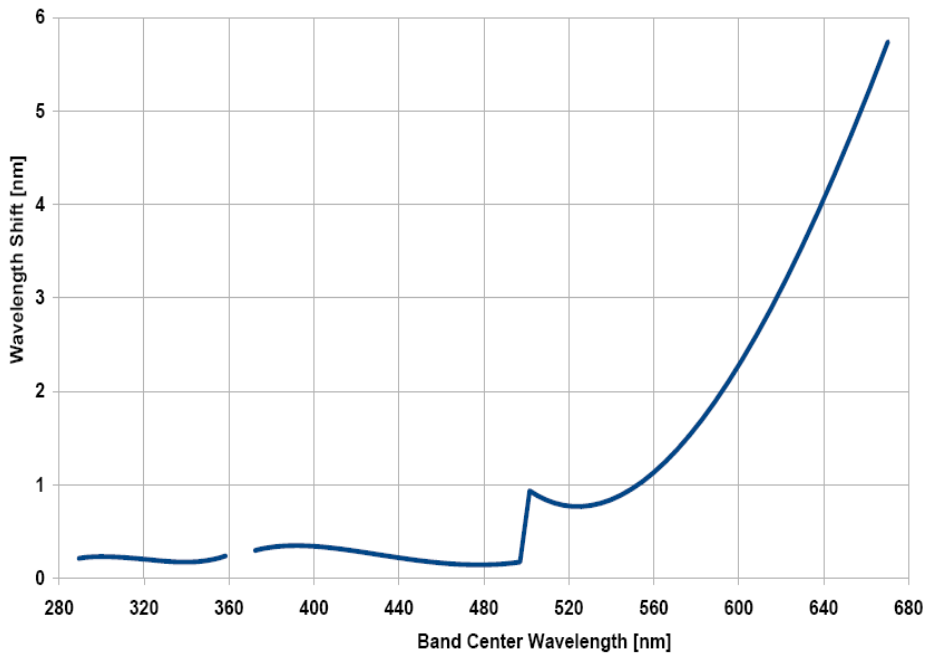

Figure 4.3: Center slit shift in band center wavelengths compared to pre-launch characterizations. Both pre-launch and post-launch measurements are characterized by polynomials, hence the smooth nature of the difference. This is also the cause of the discontinuity near 500 nm.

Regressions involving the solar backscattered spectrum are not usually as accurate as those using the direct spectrum because of increased noise and atmospheric absorption. However, we have discovered that radiances in the range 370-430 nm originating from very low in the atmosphere are quite similar in their spectral dependence to measured solar irradiances. As seen in Figure 4.4, these backscattered radiances can be fit to a reference solar spectrum as well as a solar measurement. This observation means it is possible to monitor wavelength shifts between the weekly solar measurements with high precision.

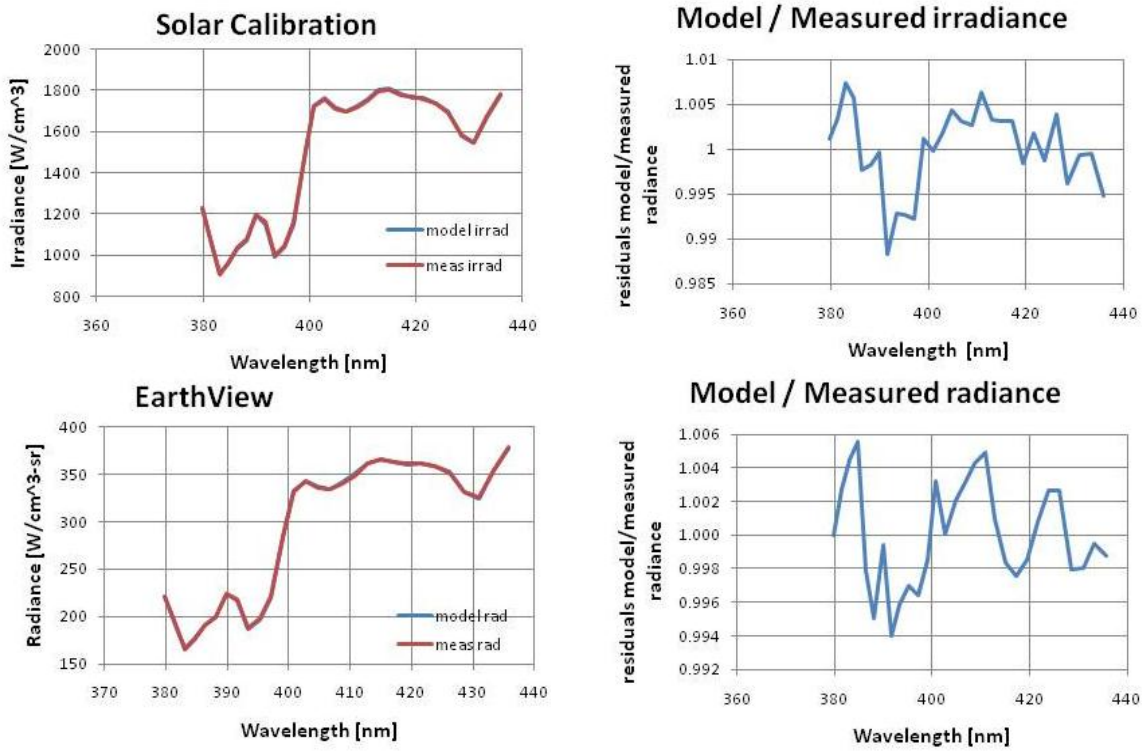

Figure 4.4: Center slit shift comparisons between measured spectra and a reference solar spectrum. The top row are comparisons with an OMPS measured solar spectrum. The plot on the right shows the observed difference after regression for a wavelength shift. A similar difference for backscattered radiance in the lower right panel is of equal or better quality.

4.4 Thermal Effects

An evaluation of pixel band center wavelengths in the earliest post-launch solar measurements revealed exceptionally large shifts compared to pre-launch measurements. While the observed shift in the Right Slit approached 1 spectral pixel, the shift in the Left Slit was almost zero. Furthermore, we discovered the band center wavelengths changed significantly during each orbit. An example of this change in the Right Slit, large aperture image is shown in Figure 4.5. The band center wavelengths remain relatively stable until approximately 2/3 of the way into the orbit. The observed shift in the Left Slit is similar, but in the opposite direction. These unexpected shifts account for the large Left-Right differential observed in the solar results, because the OMPS solar measurement is performed at the end of the orbit where the effect reaches its maximum.

The OMPS sensor vendor, Ball Aerospace, concluded that the shifts are likely caused by mechanical stress on the 6 secondary telescope mirrors. These mirrors, seen on the left side of Figure 2.3, are responsible for steering the image of each slit onto the focal plane. Any motion of these images in the dispersion direction (the narrow dimension of the slit) causes light to fall on different spectral pixels and thus appear as a spectral shift. As the subsatellite point

approaches mid-northern latitudes the spacecraft deck ceases to shade the Limb sensor from sunlight, and the solar baffle in front of the entrance apertures begins to heat up rapidly.

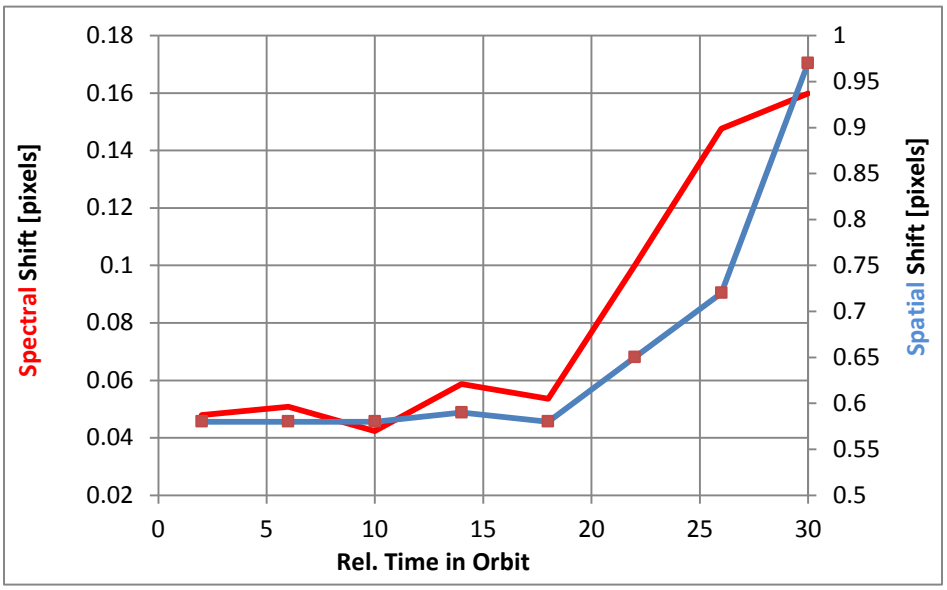

Figure 4.5: Shifts in the focal plane location where photons strike as a result of thermal-mechanical stress on the secondary telescope mirrors. In this example, shown for the Right Slit, large aperture, translations along the spatial dimension of the detector are shown in blue and along the spectral dimension are shown in red.

The thermal expansion of this baffle results in static forces on the adjacent sensor housing, the part that contains the telescope secondary mirrors. The resulting rotation of these mirrors causes a shift in the slit images at the focal place as shown in Figure 4.6.

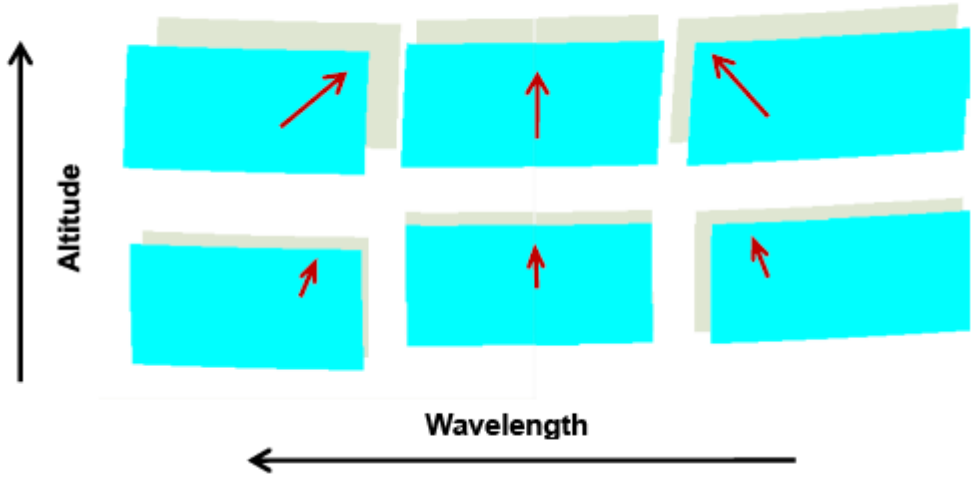

Figure 4.6: An exaggerated representation of slit image motion on the detector resulting from mechanical stresses on the 6 secondary telescope mirrors.

As seen in Figure 4.6, the mirror motion causes the focal plane images to shift in the spatial as well as the spectral direction. Unlike the wavelength shift, the resulting altitude shift is in the same direction, though not the same magnitude, for all images. Monitoring the position of solar Fraunhofer lines, described above, allows us to monitor slit image positions in the spectral dimension. We also developed a method for tracking the position of each slit's image in the spatial dimension. In a mechanically stable instrument the location of the 6 images on the detector should remain fixed. Since these images all fit within the active detector area there are large numbers of pixels that receive no photons except a small amount of stray light. A sharp signal gradient representing the bottom edge of each slit was seen moving along the spatial direction of the detector, thus confirming the predicted behavior.

The observed change in the slit edge position of the Right Slit as compared with pre-launch measurements is shown in Figure 4.5. Note that a significant change occurs at approximately the same point in the orbit as that observed for the wavelength direction. Note also there is a 0.6 pixel shift even in the early portion of the orbit, where the instrument is still in thermal equilibrium. Because the sensor temperature is at least 10 ºC cooler in orbit than it was during on-ground tests, it is likely that the forces affecting the secondary mirrors have changed permanently from when the sensor pointing was calibrated on the ground. This 0.6 pixel shift means that the Tangent Height calculated from spacecraft attitude and ephemeris is at least 0.6 km higher than it should be.

5 Altitude Registration Error

The limb-viewing techniques usually produce ozone density vs altitude profiles. To determine ozone profiles within 5% accuracy one needs to know the altitude of the tangent point (TP), called tangent height (TH), with an accuracy of about 200m, which translates into attitude knowledge of 16 arc seconds at the location of the instrument. Though star-trackers, now deployed on most modern S/C can achieve higher accuracy, the attitude must be measured close to the instrument since a large S/C bus can flex due to thermal effects caused by changing earthshine along the orbit. This is not the case for LP since the NPP star-tracker is close to VIIRS. In addition one needs to consider error in alignment of the focal plane of the instrument with respect to S/C axes. Such alignment errors can far exceed 16 arc sec.

To solve this problem a technique called Rayleigh Scattering Altitude Sensing (RSAS) was proposed two decades ago. This novel technique takes advantage of the fact that at 350 nm, where the atmospheric absorption is small and Rayleigh scattering is large, the atmosphere becomes so opaque at lower altitudes (<20 km) that one cannot see the TP. Hence, LS radiation becomes insensitive to TH. However, at 30 km and above the atmosphere is thin enough that the LS radiation decreases by ~14%/km, same as the atmospheric density. Based on both radiative transfer calculations and OMPS LP measurements, the 30 km/20 km radiance ratio (RR) varies by ~11%/km. Thus, by comparing the measured RR with the calculated values one can estimate the TH error. The primary source of error in this procedure is in calculating the RR since the LP can measure the RR to better than 1%. Since calculated RR is proportional to the ratio of pressure (P) and temperature (T) near ~30 km altitude, one needs to know this ratio to within 2% to achieve 200m TH registration accuracy. It is not known whether NCEP data that we are using for estimating P and T can provide such accuracy. The RSAS technique is also affected by aerosols above ~25 km. Currently, we are using aerosol climatology derived from historical SAGE data to do the aerosol correction. If we assume ±50% error in the actual aerosol amount with respect to climatology, an error in TH estimated from RSAS can vary from ±100m in the

southern high latitudes, ±300 m in the tropics, to ±500m in the northern high latitudes. We may be able to reduce this error by using the aerosol profiles derived from OMPS LP, but this will take some time.

Although the effect of DUR, which we discussed in Section 3, mostly cancels out in computing the RR, the cancellation is imperfect if the albedo of the scene underneath the TP varies along the LOS. Because of the high opacity of the atmosphere at 20 km, the LS radiation is most affected by clouds that are several hundred km away from the TP towards the satellite, while radiation at 30 km is most sensitive to clouds under the TP. So, the RR is affected by gradient in cloud albedo under the LOS rather than by cloud albedo itself. The method works better in higher latitudes where the underlying scene tends to be relatively more homogeneous than in the tropics. Larger solar zenith angles also help since the cloud effect reduces as cosine of solar zenith angle.

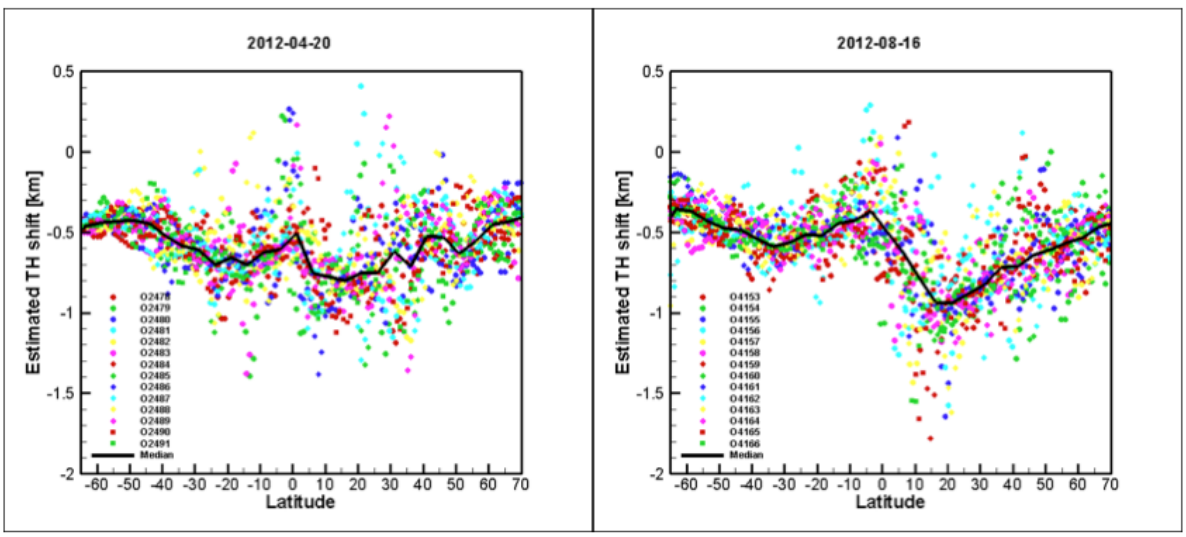

Figure 5.1: Tangent height correction estimated using the radiance ratio-based RSAS method described in the text. The noise in the tropics is due to gradient in cloud albedo along the line of sight and aerosols. The thick solid lines are the median values in each 10˚ latitude band.

Figure 5.1 shows the TH correction (THC) estimated for two days using the RSAS method described above. Most of the noise in the tropical altitudes is probably due to inhomogeneity in cloud albedo, though variations in aerosols and errors in P/T ratio derived using NCEP data may also be contributing factors. Though the data from the two days are not identical the broader patterns are similar. The global mean value of THC is -700m ±300 m. This error is in addition to -1.35 km THC that has already applied in the data shown in Figure 5.1. Though there is an indication of variation in THC with latitude, we are not yet sure whether this is a real variation in the S/C pitch at OMPS LP location or due to uncertainties in the RSAS method.

We have attempted to validate the RSAS results shown in Figure 5.1 by comparing OMPS and MLS ozone profiles. Unfortunately, it is not possible to do apples–to-apples comparison between these sensors. MLS ozone profiles are reported as mixing ratio (MR) vs pressure while

OMPS profiles are reported as density vs altitude. To compare the two profiles we had to convert MLS MR profiles into density profiles using MLS provided temperature and geopotential heights (GPH). Though the MLS temperature profiles are of very high quality, the MLS team has indicated that their GPH profiles may have errors of up to 200m at 100 hPa and the errors may increase with altitude. It is, therefore, not clear if MLS/OMPS comparisons can provide better estimate of TH error than the RSAS method.

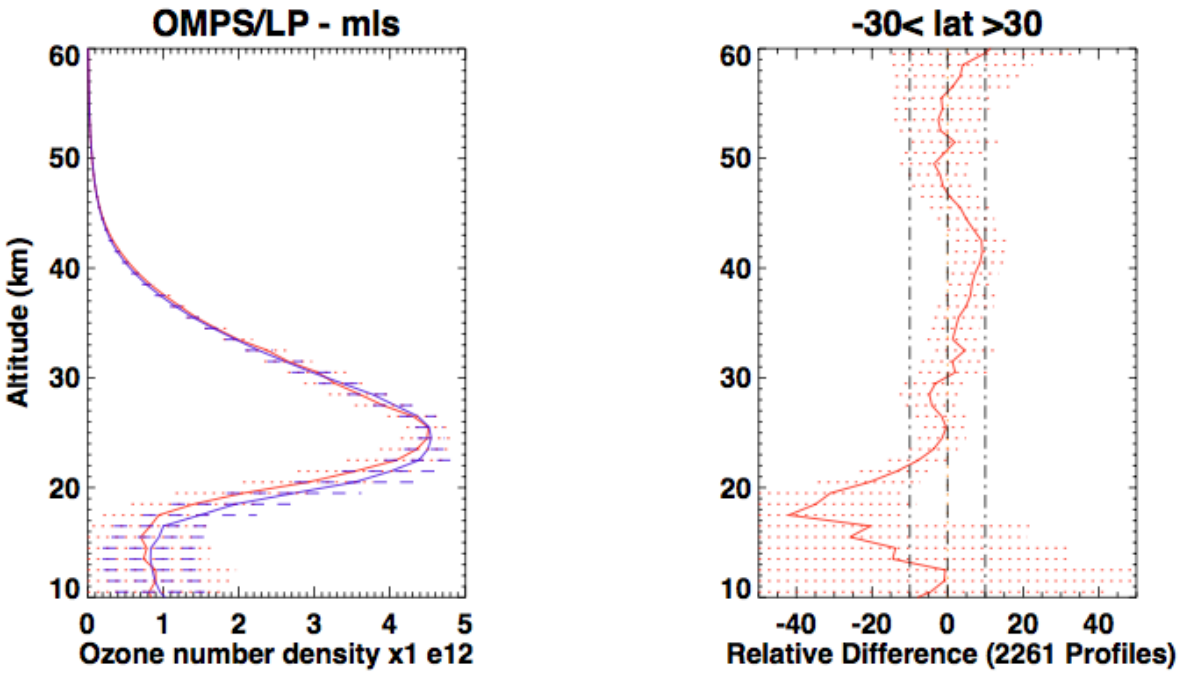

Figure 5.2: Comparison of MLS and OMPS-LP ozone density profiles for a tropical latitude band. MLS mixing ratio profiles were converted into density profiles using MLS temperature and GPH profiles, which introduces added uncertainties in MLS profiles. One sees ~1 km shift between the two profiles below the ozone density peak but much less above the peak, indicating that there are other errors involved besides altitude registration error.

Figure 5.2 shows a typical comparison between MLS and OMPS profiles for the tropical region. While one sees a very clear ~1 km shift between the two profiles below the ozone density peak, nearly identical to the RSAS estimates, the shift above the peak is less well defined and smaller. This implies that there are other errors besides TH that are affecting the comparisons.

6 Evaluation of OMPS LP ozone profiles

The Microwave Limb Sounder (MLS) was launched on the EOS Aura satellite in July 2004. It is currently producing one of the best datasets of ozone profiles available from any source. Therefore, for evaluation of OMPS LP ozone profiles we will focus primarily on this dataset. However, as we noted in Section 5, OMPS profiles are retrieved in density vs altitude coordinate while MLS profiles are provided in volume mixing ratio (VMR) vs pressure coordinate. Since most users prefer the latter coordinate, we convert OMPS density profiles into VMR profiles using assimilated temperature and geopotential height data from NCEP. We will focus primarily on these converted VMR profiles. However, we have not evaluated OMPS LP mesospheric VMR profiles since mesospheric NCEP data are not reliable. In the next release we are planning to switch to GMAO data from NASA GSFC to improve OMPS VMR profiles in the mesosphere.

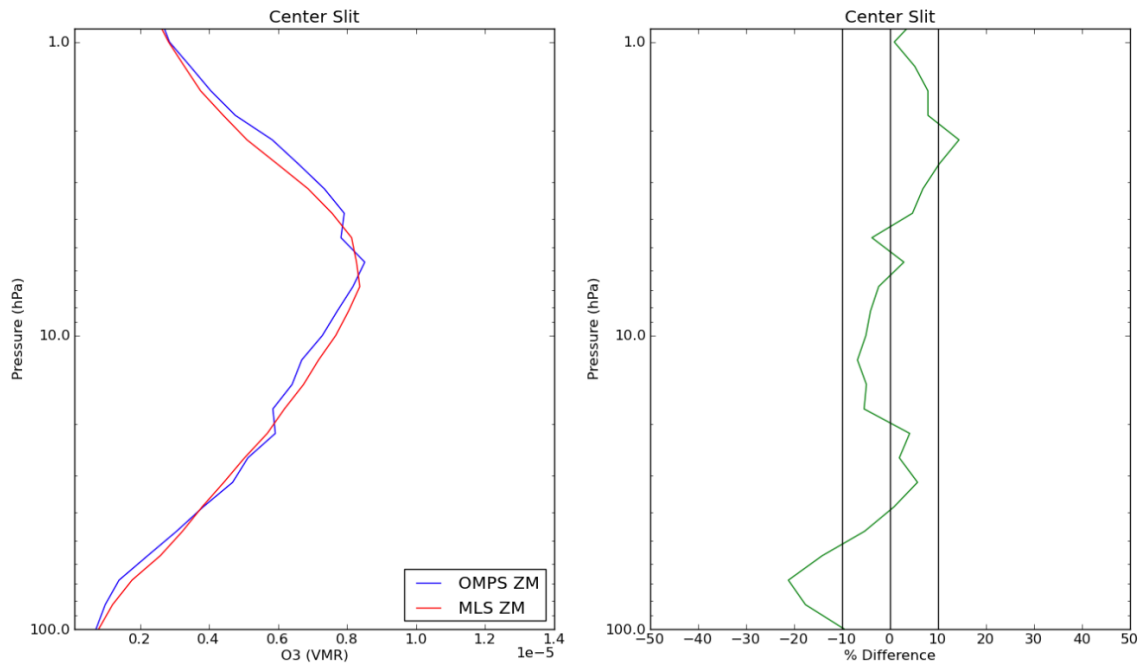

Figure 6.1: Monthly zonal mean ozone profiles at 45˚N (April 2012) from OMPS and MLS are compared in the left panel. The panel on the right displays the percent difference.

Figure 6.1 shows comparison of 45˚N monthly zonal mean profiles from MLS and OMPS for April 2012. The two sensors are mostly within 10% except in the lower stratosphere. One notes that the OMPS profile has vertical structures while the MLS profile is smooth. These structures are not caused by instrument noise since the profiles shown are averages of several hundred individual profiles. Recent analysis suggests that these structures are largely due to insufficient vertical smoothing applied in the retrieval algorithm. This is not uncommon since algorithms developed prior to launch usually assume spectrally uncorrelated random measurement errors. Real instruments often have correlated errors that are not easy to model. In the next release we plan to adjust the smoothing parameters to minimize the impact of such errors.

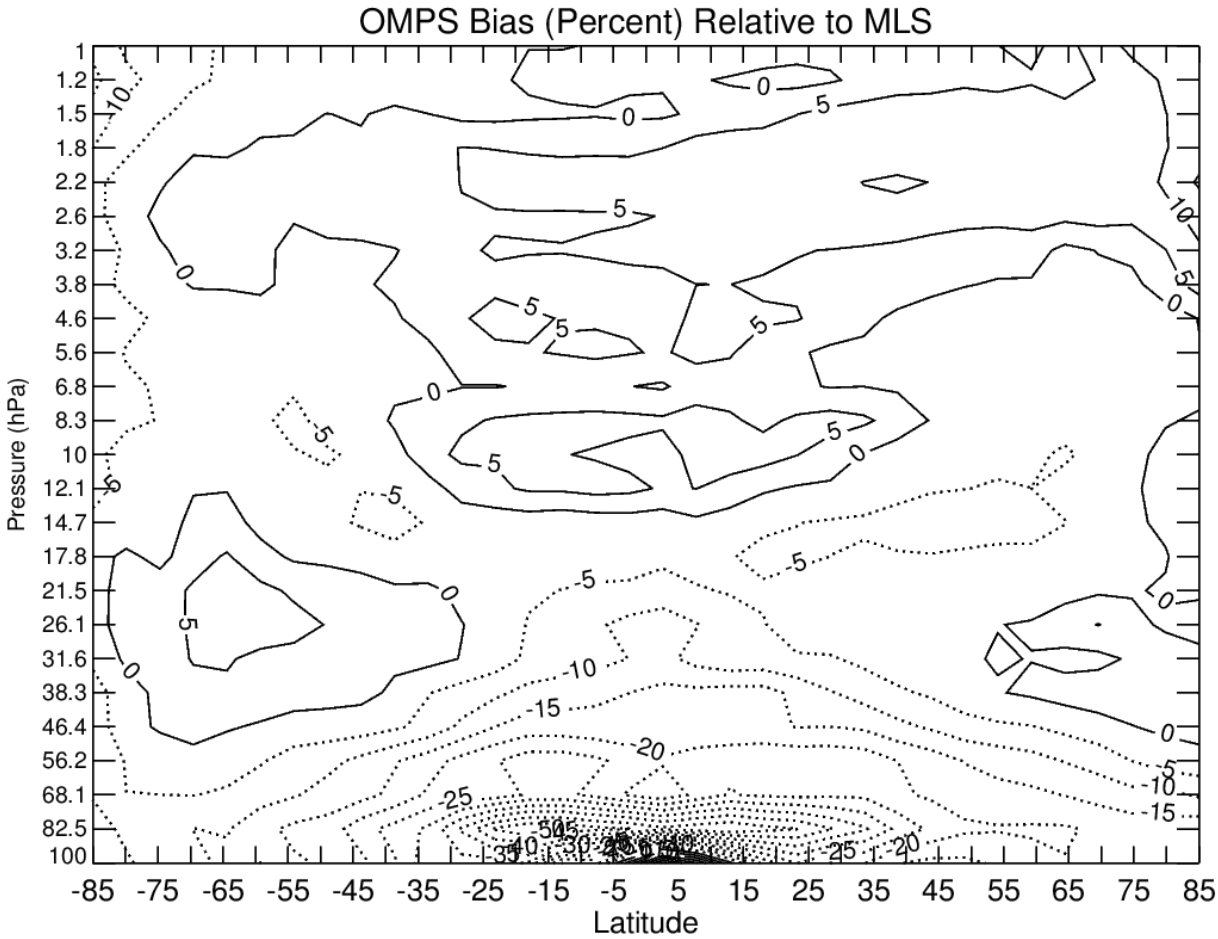

Figure 6.2: Percent difference between OMPS and MLS zonal mean ozone profiles as a function of pressure and latitude. Nine months of MLS and OMPS data (March-November 2012) were averaged for these comparisons.

In Figure 6.2 we show a contour map of percent difference between OMPS and MLS monthly zonal mean profiles as a function of latitude and pressure. Nine months of MLS and OMPS data (March-November 2012) were averaged for these comparisons. Again we note that the differences between the two instruments are mostly within 10% except in the lower stratosphere. Differences in the lower stratosphere will greatly reduce in the next release when we apply an additional -650 m adjustment to TH based on RSAS analysis, as we discussed in the last section. However, the adjustment will produce a negative 5-10% bias in the upper stratosphere. This could be partly due to error in the NCEP data.

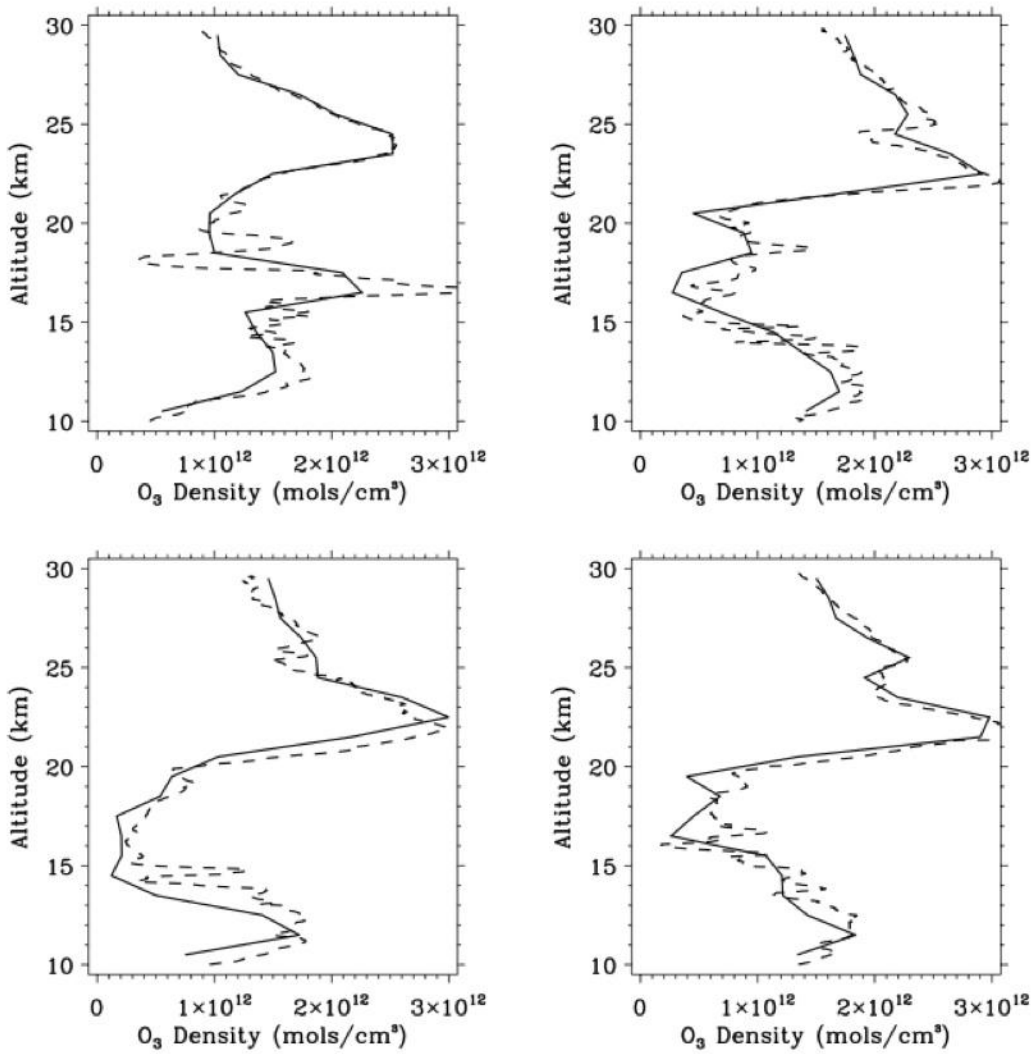

Figure 6.3: Individual ozone profile comparisons between OMPS (solid line) and ozonesondes (dashed line) launched from the German Antarctica station Neumayer (71˚S, 8˚W) during the time period of the 2012 ozone hole formation.

In Figure 6.3 we show comparison with 4 ozonesonde profiles measured from the German Antarctica station Neumayer (71˚S, 8˚W) during the time period of ozone hole formation. We show these comparisons in density vs altitude coordinate since sondes provide such data. The comparisons show that OMPS LP can capture much of vertical structures that sondes see, but not all. Such differences are commonly seen when one compares an in situ instrument that samples local air with a remote sensing instrument that averages over several hundred km horizontal distance.

7 Path Forward

7.1 Data Release #2

We plan to reprocess the entire OMPS-LP data record, both L1b and L2 data, later this year. The exact date for the next release will depend upon progress toward the necessary modifications. The following provides a summary of the changes that we plan to implement. We will consider making other changes if the time permits.

1. Correction for thermal effects: As we have discussed in Section 4.4 images of the limb on the detector have shifted both in the spectral and vertical dimensions since launch. And they shift along the orbit as the sunlight warms up the front optics in the northern hemisphere. This effect is well understood and we plan to correct it.

2. Altitude Registration: We have reasonably convincing evidence, from both RSAS analysis and MLS comparisons, that there is ~100 arcsec error in the pitch direction pointing of the sensor boresight relative to the S/C master reference. We plan to correct this one-time error. Although there is an indication of additional ±20 arcsec variations in the knowledge of LP pointing along the orbit, we do not yet have enough confidence in our estimates to apply a correction in the next processing.

3. Increased Smoothing Parameter: Daily zonal mean ozone profiles from OMPS LP have high resolution vertical structures that are clearly not geophysical. We have found that these structures can be reduced by increasing the smoothing parameter assumed in the inverse model. We plan to adjust the smoothing parameter in the next processing.

4. Remove OH contaminated wavelength: We have found that the OMPS LP measured radiances near 309 nm are contaminated by airglow produced by hydroxyl radical (OH). Since this contamination has strong altitude dependence, it produces an error in the ozone retrieval. We plan to delete these wavelengths from ozone processing.

5. Based on demands from users, we plan to release the aerosol product that comes out of the current L2 S/W. However, we note that this product will be provided as is. The OMPS limb team currently doesn't have the resources or expertize to create a validated scientific product of aerosols. This is the only new product release planned.

6. The OMPS limb data are affected by transients, most notably due to the effect of charge particles in the South Atlantic Anomaly (SAA). We plan to develop a scheme to flag and possibly remove such bad data.

7.2 One Year and Beyond

There are several known issues with the data system that we will not be able to fix by release #2. They are listed here.

1. OMPS limb data are collected on-board using a sample table that specifies the pixels on the CCD for which data are downloaded. This table should be refined to more efficiently use the limited data rate available to OMPS. For example, there may be little advantage to retrieving high altitude ozone for all 3 slits.

2. The radiance gridding and consolidation S/W in the L1b code produces vertically and spectrally gridded radiances and combines measurements from different gain settings (Section 2.2). This S/W is not as robust as it should be. We plan to separate the gridding portion of the

process that the L2 S/W currently requires from the problematic consolidation process. We will investigate improvements to consolidation and possibly eliminating it entirely. Retrievals may be possible using only large or small aperture radiances. We will also examine if it is worth modifying the L2 S/W to accept un-gridded radiances.

3. We plan to replace the current inversion technique based on Twomey-Tichonov regularization scheme with the optimal estimation (OE) method. In the OE method the vertical resolution of the retrieved profile is optimized based on the known variability of the atmosphere. Therefore, more smoothing is applied at altitudes where the atmosphere is relatively quiet and vice-versa.

4. Improvement to tangent height registration. While we will continue to refine and improve the RSAS scheme described in Section 3, we are looking at other methods of improving our altitude registration. One promising method is to take advantage of the fact that the reflectivity of the underlying scene derived from OMPS LP measurements is very sensitive to small errors in altitude registration. Since the OMPS LP reflectivity should on average agree with the reflectivity derived from nadir sensors (OMPS NM and VIIRS), we should be able to estimate altitude registration errors by comparing reflectivities. Another method that shows promise involves detecting the location of the lunar limb and comparing with predictions.

5. The L2 software currently produces residuals- differences between measured radiances and radiances simulated using the retrieved ozone, reflectivity and aerosol profile- that are much larger than instrument noise. This usually implies that there are systematic errors in the measured or calculated the radiances. Errors in simulating the radiances can come from the radiative transfer code (forward model) or from ancillary data, viz., temperature and pressure profiles from NCEP. If the problem can be isolated to NCEP, we have a potential method of retrieving temperature profiles from LP data. This technique is most promising above 35 km where meteorological sensors do not provide good temperature information.

6. As we noted in Section 3, the OMPS LP has the potential of providing somewhat better ozone profiles than other limb sensors below the ozone density peak. We will continue to explore methods of achieving this goal.

7. OMPS-LP takes more measurements in a given latitude band than most limb sensors flown so far. This can help minimize cloud contamination to sample the upper troposphere (UT). Though it is non-trivial to derive reliable ozone and aerosol profiles in the UT region, we are hopeful that with further work the OMPS LP will be able to do so.

8 Recommendations

In this section we provide few recommendations that can be used in planning the organization of the future OMPS science team.

The three OMPS sensors must be operated together as a suite. We think that there is good synergy between the three sensors that can only be exploited if there is a single team that processes the data, calibrates the instruments, and implements algorithms designed to take advantage of this synergy. Hence we recommend that there should be a single science team for OMPS with a team leader tasked to foster the synergy. Some examples of this synergy are discussed below.

1. OMPS data processing currently relies upon RDR products generated within NOAA's IDPS. Processing of the raw (Level 0) data by IDPS provides no added value, and often introduces

unnecessary delays and data loss. The Ozone PEATE is currently capable of processing Level 0 data directly from the ground station, and we prefer that approach.

2. Many of the tools and software developed for Limb sensor operations and data processing also support NASA's Nadir sensor effort. These sensors have common flight electronics and identical detectors, so much of the ground software through Level 1 is shared. We believe it is in NASA's best interest to provide OMPS calibration and Level 1 data production as a common resource to the science teams selected for OMPS.

3. The OMPS nadir mapper (NM) can greatly improve its science return by collecting data at higher spatial resolution. Since the combined data rate allocated to OMPS is fixed, one will have to trade the data rate between the limb and nadir sensors to optimize the science return from both sensors.

4. All three OMPS sensors are capable of providing ozone profiles. The OMPS NM is most sensitive to tropospheric ozone profile, while the OMPS LP is most sensitive to the stratosphere. Therefore, these two instruments working together can provide both stratospheric and tropospheric ozone profiles, something that has not been achieved from any previous sensor flown in space. OMPS NM can help in inter-calibrating the two sensors and for tying the OMPS measurements with long-term ozone record from SBUV sensors that goes back to 1970. Several SBUV/2 sensors continue to operate on NOAA polar satellites.

5. The OMPS NM has excellent information about volcanic ash and sulfur dioxide. The latter quickly converts into sulfate aerosols. It can also detect smoke plumes that sometime get injected into the upper troposphere and lower stratosphere (UTLS) by deep convection. OMPS limb can detect these aerosols with very high sensitivity and can provide altitude information. Recent results show that OMPS LP has very high sensitivity to meteoritic dust whose contribution to the stratospheric aerosol layer is not well understood. So the two sensors working in combination can provide a rich source of aerosol data in the UTLS region for climate studies.

6. Based on experience with SBUV sensors we know that OMPS nadir profiler (NP) should have good information about polar mesospheric clouds (PMC). OMPS LP can provide good estimate of the height of these clouds and can detect thinner clouds. The two sensors working in combination can continue the record of PMCs that has been created by NASA’s AIM satellite. PMCs are considered an important marker of climate change.